photonics

MDPI

Article

Generation of Different Mode-Locked States in Nonlinear Multimodal Interference-Based Fiber Lasers

Gang Deng [1,2], Qiaochu Yang [1,2], Silun Du [1,2], Bowen Chen [1,2], Baoqun Li [1,2] and Tianshu Wang [1,2,*]

[1] National and Local Joint Engineering Research Center of Space Optoelectronics Technology, Changchun University of Science and Technology, Changchun 130022, China; dgcw@mails.cust.edu.cn (G.D.); yangqc@cust.edu.cn (Q.Y.); silundu@mails.cust.edu.cn (S.D.); 2020200057@mails.cust.edu.cn (B.C.); libaoqun@mails.cust.edu.cn (B.L.)

[2] College of Opto-Electronic Engineering, Changchun University of Science and Technology, Changchun 130022, China

* Correspondence: wangts@cust.edu.cn

Abstract: A novel mode-locking method based on nonlinear multimode interference (NLMI) using a distributed large-core (105 μm) graded-index multimode fiber (GIMF)-based saturable absorber (SA) capable of generating four pulse modes is proposed. The distributed SA geometry consists of two GIMFs located at different positions in the resonant cavity. The coupling and joint operation not only facilitate resistance to pulse fragmentation but also provide a sophisticated and widely tunable transmission with saturable and reverse saturable absorption phenomena. Based on this, dissipative soliton (DS), dissipative soliton resonance (DSR), wedge-shaped, and staircase pulses are achieved without additional filters. The DS has accessible output power, pulse energy, bandwidth, and duration of up to 15.33 mW, 2.02 nJ, 22.63 nm, and ~1.68 ps. The DSR has an achievable pulse duration and energy of ~32.39 ns, 30.3 nJ. The dispersion range that allows DS operation is studied, and the dynamics of the evolution from DS to DSR are observed. The versatility, flexibility, and simplicity of the SA device, combined with the possibility of scaling the pulse energy, make it highly attractive for ultrafast optics and nonlinear dynamics.

Keywords: nonlinear multimode interference; graded-index multimode fiber; mode-locking; coupling transmission; nonlinear dynamics

check for updates

Citation: Deng, G.; Yang, Q.; Du, S.; Chen, B.; Li, B.; Wang, T. Generation of Different Mode-Locked States in Nonlinear Multimodal Interference-Based Fiber Lasers. *Photonics* **2024**, *11*, 216. https://doi.org/10.3390/photonics11030216

Received: 2 January 2024
Revised: 25 January 2024
Accepted: 5 February 2024
Published: 27 February 2024

Copyright: © 2024 by the authors. Licensee MDPI, Basel, Switzerland. This article is an open access article distributed under the terms and conditions of the Creative Commons Attribution (CC BY) license (https://creativecommons.org/licenses/by/4.0/).

1. Introduction

All fiber-format passively mode-locked (ML) laser systems have attracted considerable attention due to their wide range of applications in industry and scientific research [1]. Various material-based real SAs have been developed to actuate mode locking, such as semiconductor saturable absorption mirrors [2], single-walled carbon nanotubes [3], graphene [4], transition metal chalcogenides [5], topological insulators [6], black phosphorus [7], etc. However, these materials often have a fixed transmission and suffer from optical power-induced thermal damage and oxidation, which restricts the damage threshold and long-term stability. Physically, non-linear phenomena can also achieve intensity modulation, known as "saturable absorption", which can discriminate against low-power signals and leave high-power ones with minimal influence [8]. One feasible option is to manipulate the nonlinear effects in the fiber to obtain an artificial SA, such as nonlinear polarization rotation (NPR) and nonlinear amplifying loop mirror (NALM) [9,10], etc. In fact, SAs with all-fiber structures have the advantage of being compact and less susceptible to damage than real SAs. Inspired by this vision, researchers from different communities are trying their best to further develop new types of SAs.

Recently, GIMFs with a larger mode area have experienced a strong resurgence as a scientific frontier due to higher power handling capabilities and intriguing nonlinear optical properties (e.g., self-phase modulation, cross-phase modulation, and four-wave mixing,

etc.) [11,12]. This makes them an ideal platform for studying various complex nonlinear dynamics. Numerous nonlinear phenomena, such as spatial beam cleaning, spatiotemporal instability, especially the NLMI self-imaging effect, have been observed and studied [13]. As light is coupled from SMF into GIMF, multiple high-order modes will be excited in the GIMF. The multimode interference effect between modes leads to the self-imaging phenomenon. Around 2013, Mafi et al. theoretically proposed that the single-mode fiber (SMF)-GIMF-SMF structures, based on NLMI, have intensity discrimination of the modes due to different amounts of Kerr effect and can be used as an effective SA and filter [14]. Subsequently, such an approach has been demonstrated experimentally [15–21]. Researchers solved the problem of the strict length limitation through several innovative methods such as adding a segment of step-index multimode/no-core fiber ahead of the GIMF [22–25], introducing an inner micro-cavity in the GIMF [26], stretching the GIMF [27–29], offset-splicing the GIMF [30,31], coiling the GIMF [32], etc. Through these methods, more high-order modes in the GIMF can be excited, and the mode field distribution can also be reconstructed, both of which lead to a reshaping of the transmission, thus removing the length limitation of the GIMF. Among them, Li et al. experimentally confirmed that the GIMF–SA could be a perfect combination of SA and filter [20,21,28,29]. These results indicate that the possibility of strong spectral filtering arising from such an SA can provide suitable amplitude modulation in support of chirped pulses and play a vital role in managing competition without blocking components. Chen and Dong et al. experimentally demonstrated that the transmission curve of the GIMF-based SA has sinusoidal-like oscillatory properties with saturable and reverse saturable absorptions [16,30]. These findings suggest that the transmission characteristics of the GIMF-based schemes are rich, complex, and adjustable, thus facilitating versatile high-energy ML operations. Obviously, an NLMI-based modulator possesses the advantages of higher power tolerance, simplicity, and near-instantaneous response. Thus, NLMI lasers hold the promise to produce high-energy, highly chirped, DS, and dissipative-class rectangular pulses with an all-fiber architecture. Although the GIMF–SA is an effective method for soliton generation, research on NLMI-based all-fiber lasers is still in its infancy, and the performance is seriously deficient, with ML operations usually limited to no more than two kinds ($N \leq 2$) and pulse energy in the sub-nJ level. To date, most studies have focused on condensed splice structures; the coupling characteristics and joint action of two discrete homogeneous GIMFs have not been addressed in previous reports. In addition, to the best of our knowledge, there are few reports on the operation of DSR within the communication window (1.55 μm) using the reverse saturable absorption phenomenon of distributed GIMF–SA.

In this letter, we propose and experimentally demonstrate a distributed 105 μm large-core GIMF architecture, which provides simultaneous SA and spectral filtering operation. The large-core GIMF device not only facilitates expansion of the model field and resistance to pulse fragmentation but, more interestingly, the coupling and joint action provide more complex, richer, and widely tunable transmission properties with saturable and reverse saturable absorption. Using such a device, a simple and compact all-fiber passive ML laser can be built without bulk filters, and in addition, four ($N = 4$) ML operations, including DS, DSR, wedge-shaped, and staircase pulses are generated. The DS has an accessible output power, pulse energy, bandwidth, and duration of up to 15.33 mW, 2.02 nJ, 22.63 nm, and ~1.68 ps. The DSR has an achievable pulse duration and energy of ~32.39 ns, 30.3 nJ. Furthermore, the evolution from DS to DSR is also observed, similar to the theoretical work in refs [33–35]. The distributed GIMF scheme is essentially a new way of achieving a stable, compact, high-power, multifunctional laser source that can be used in sensing, communications, etc. [36–38].

2. Experimental Setup and Principles

The experimental setup, as presented in Figure 1, is in a ring configuration. An 18 m erbium-doped fiber (EDF: absorption coefficient of 4.71 dB/m at 980 nm, OFS, MP980) is utilized as the gain medium and is core-pumped by a 976 nm laser diode (LD: maximum power

1039 mW) via a 980/1550 nm wavelength division multiplexer. A dispersion-compensated fiber (DCF: dispersion parameter of ~−38 ps/nm/km; length: 1.38 m; THORLABS, DCF38) is employed to manage the dispersion. A polarization controller (PC) is used to carefully optimize the cavity birefringence, while a polarization-insensitive isolator (PI-ISO) maintains the unidirectional operation. The distributed GIMF–SA, responsible for high multimode excitation, mode-locking, and filtering, is located upstream of the PC and downstream of the PI-ISO. Additional stretches of SMF/DCF are added in the cavity to compensate for cavity dispersion and non-linearity and a 20:80 coupler with 20% output. The initial length is approximately 27.16 m, yielding an estimated net cavity dispersion of ~0.28 ps^2 and a fundamental repetition of ~7.58 MHz. The main instruments used are an optical spectrum analyzer (OSA, YOKOGAWA AQ6370D, Tokyo, Japan), oscilloscope (OSC, Agilent-DSO925A, PaloAlto, Santa Clara, CA, USA), detector (Agilent, 8163B, PaloAlto, Santa Clara, CA, USA), RF spectrum analyzer (ESA, Agilent, N9030A, PaloAlto, Santa Clara, CA, USA), and autocorrelator (Femtochrome, FR-103XL, Berkeley, CA, USA).

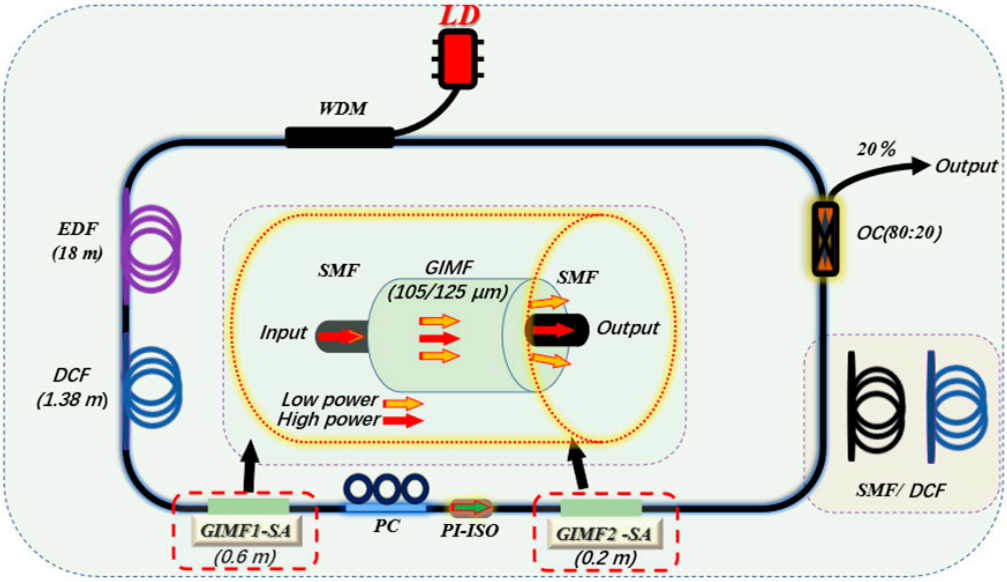


Figure 1. Schematic diagram of the distributed GIMF NLMI-based fiber laser.

We propose a distributed structure with two GIMFs of unequal length located at different positions in the resonant cavity, which introduces a variable mode field distribution and associated mode coupling ratio through an intermediate SMF that could remove the length constraint by the fusion splicer and is a variant of the offset-spliced SA in refs [30,31]. As illustrated in Figure 2a, the distributed GIMF1–GIMF2 (Fibestar: GI105/125-AC; diameter: 105 μm; numerical aperture: 0.24; and lengths: 0.6, 0.2 m), although located at different positions in the resonant cavity, act as an integral SA device. According to the theoretical model and experimental research [14,16,21,30], the transmission can be described as $T = c_0 + c_1 sin^2(I/I_{sat})$, where c_0, c_1, I, and I_{sat} denote the minimum transmission, modulation depth, instantaneous, and saturation power, respectively. In our measurement setup, a home-made NPR ML 1.56 μm pulsed laser (bandwidth of 3.77 nm and repetition rate of 17.96 MHz) is injected into the integral SA after amplification, and the transmission properties can be obtained in detail by recording the power change before and after passing through the SA in small steps. As can be seen in Figure 2b, under certain conditions, the transmission has a pronounced oscillation with saturable and reverse saturable absorption phenomena. The SA can be switched between the saturable and reverse saturable absorption regions by changing the intensity of the input light. The modulation depth is approximately 18.91% and the reverse saturable absorption power density is ~7.58 MW/cm^2. It should be noted that the transmission can vary greatly depending on the polarization state and bending pattern of the distributed SA, so this flexibility has the potential to cater

to various customizations. To achieve this, a set of heat shrink tubes of different diameters has been jacketed in the middle of GIMF1 and GIMF2, respectively. These tubes can be easily, flexibly, and finely moved, rotated, and twisted when both sides of GIMF1/GIMF2 are attached to the optical platform with adhesive tape.

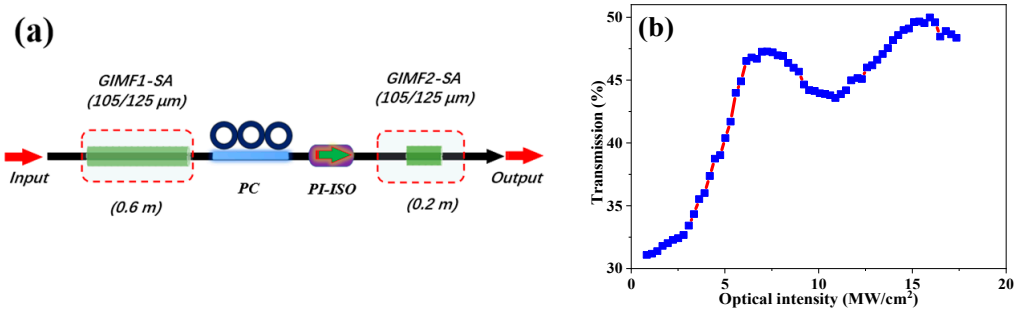


Figure 2. (**a**) Schematic diagram of the distributed SA; (**b**) measured absorption property of the distributed GIMF device.

3. Experimental Results

Initially, to verify the performance of this SA and optimize the ML state, we conducted a large-scale survey on dozens of sample sets. Figure 3 illustrates the comparative results of variable control after some rough screening. Firstly, when the length of GIMF1 is set to 0.6 m, Figure 3a shows the ML operations under the maximum lasing without pulse splitting that can be obtained by gradually cutting back GIMF2 from 1 to 0.012 m. As can be seen, mode-locking can be achieved within any length setting in this range. All spectra share the DS signature of a rectangular profile with a flat top and steep edges. The optical spectrum edge-to-edge bandwidths and signal-to-noise ratios (OSNR) range from 10.31 to 20.58 nm and 29.07 to 34.83 dB, respectively. It should be noted that the spectrum reaches its maximum bandwidth when the length of GIMF2 is in the range of 0.15–0.4 m. The insets represent the corresponding autocorrelation (AC) traces with durations ranging from 1.08 to 2.18 ps. Similarly, by gradually cutting back GIMF1 from 1.25 to 0.05 m, Figure 3b presents the accessible spectrum of ML operations at maximum pumping intensity without suffering from pulse fragmentation, with GIMF2 fixed at 0.2 m. The bandwidth and OSNR range from 11.05 to 20.58 nm and 29.82 to 35.06 dB, respectively. As can be seen, the spectrum reaches its maximum bandwidth when the length of GIMF1 is in the range of 0.85–0.45 m. The insets also illustrate the corresponding AC traces with durations ranging from 1.12 to 2.32 ps. These achievements suggest that there is essentially no limit to the length of the distributed GIMF–SA device. It should be noted, however, that an excessively long GIMF will result in increased losses and lower output, while an ultra-short GIMF will degrade stability and have low splitting thresholds. Therefore, we believe that setting the SA near ~0.6@0.2 m should be a compromise for the system and is conducive to optimizing the ML operation.

Subsequently, a detailed investigation of ML operation is implemented by setting GIMF1 and GIMF2 to 0.6@0.2 m, respectively. With appropriate adjustment of the PC, SA, and pump intensity, the DS ML operation is observed in the range of 56 to 1039 mW pump power without fragmentation. The measured evolution of the optical spectrum is presented in Figure 4a, and the central wavelengths are ~1559.39−1559.46 nm (resolution: 0.02 nm). They all have a typical rectangular profile with a flat top and sharp edges, and the edge-to-edge spectral width ranges from 16.07 to 22.63 nm. Note that the OSNR varies from 28.21 to 33.65 dB, indicating a high quality of DS operation. The radio frequency (RF) measured with a resolution of 100 Hz without residual sidebands is located at ~7.58 MHz, which matches well with the cavity, as shown in Figure 4b. A signal-to-noise ratio (SNR) of ~60.76 dB confirms stable operation and low timing jitter. The inset exhibits a 300 MHz RF spectrum. Figure 4c exhibits the AC trace at ~1.68 ps duration for a Gaussian assumption. Thus, the time bandwidth product (TBP) is ~4.69, indicating that the DS ML pulses are

highly chirped. The inset presents a pulse train with a separation of 131.93 ns. The linearly approximated varying output power given in Figure 4d ranges from 0.78 to 15.33 mW versus pump power, corresponding to a pulse energy range of 0.1–2.02 nJ and a peak power of ~1.2 kW. Thanks to the large-core GIMFs and associated coupled transmission, single-pulse operation can be maintained over such a wide range without suffering from pulse fragmentation. Physically, unlike conventional solitons that originate in a Hamiltonian system, DS is formed by a compromise of gain, loss, dispersion, non-linearity, and strong spectral filtering. As mentioned above, the TBP ranges from 2.33 to 5.59, indicating that the chirp is not only strong but also highly variable. In the present laser, the guiding of the pulse evolution by converting the pulse chirp into self-amplitude modulation can be attributed to the distributed GIMF structure with a filtering property, considering that no additional filter components are inserted [20,21,26,28]. Thus, the GIMF device functions as both SA and filter. In addition, during our experimental observations, the laser could achieve self-starting if the oscillator is undisturbed.

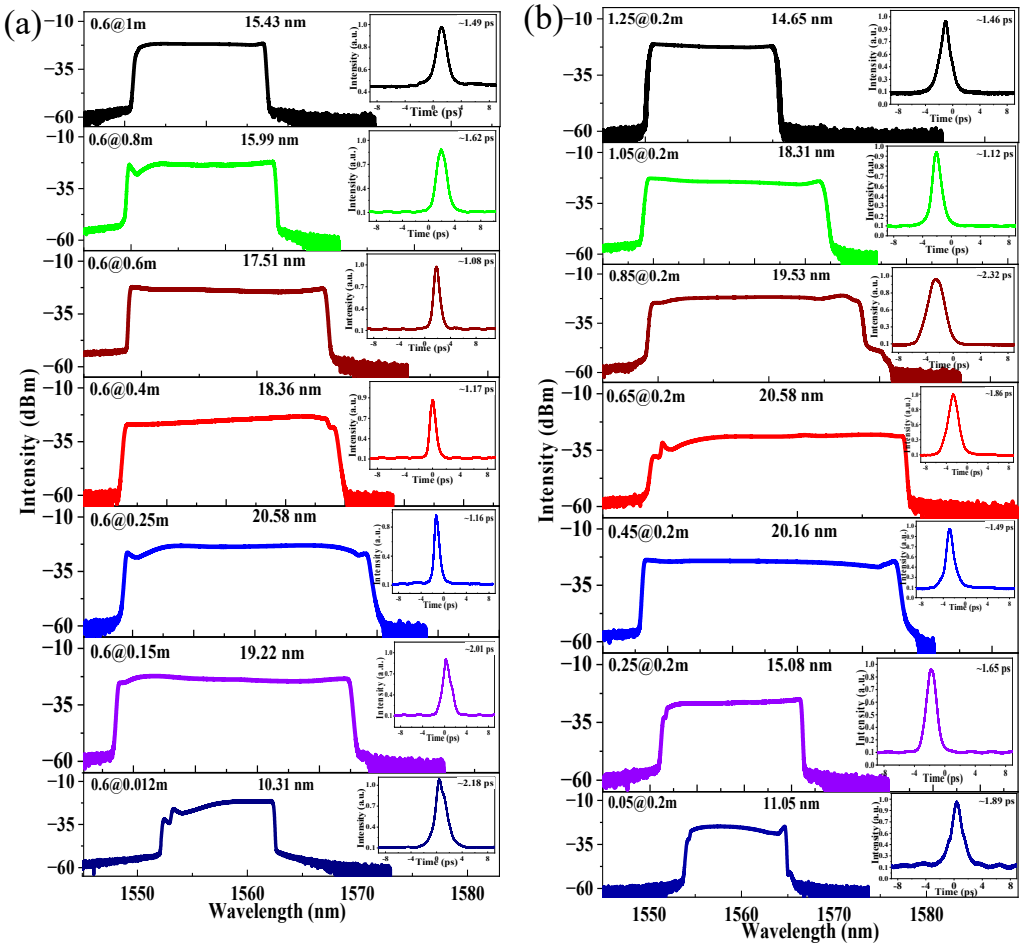


Figure 3. Characteristics of the DS operation of various samples. (**a**) The achievable spectrum versus GIMF2 when GIMF1 is fixed at 0.6 m. Insets present the corresponding AC traces; (**b**) the achievable spectrum versus GIMF1 when GIMF2 is fixed at 0.2 m. Insets present the corresponding AC traces.

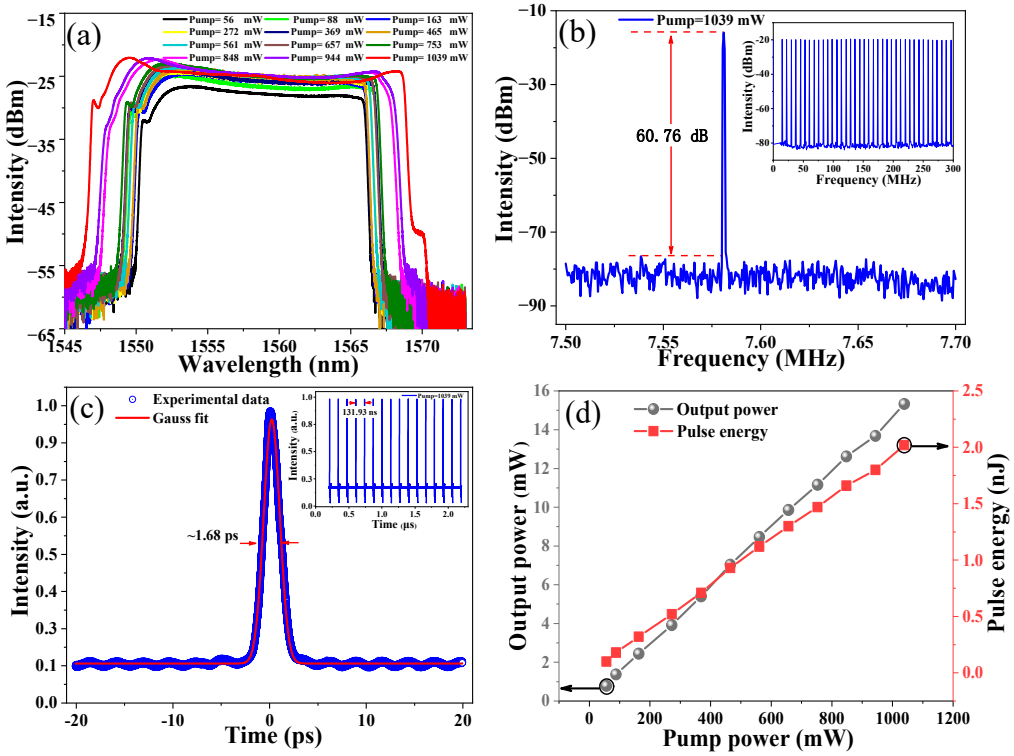


Figure 4. Characteristics of the DS operation. (**a**) Optical spectrum; (**b**) RF spectrum at 1039 mW pump power. Inset: the RF spectrum for a 300 MHz span; (**c**) the corresponding AC trace. Inset presents a pulse train; (**d**) the output power and pulse energy versus the pump power.

As a novel approach to mode locking, it would be interesting and worthwhile to investigate the performance of this distributed GIMF–SA at different dispersions and to find out the range of dispersions in which DS could exist. Therefore, we chose to determine the lower boundary of the dispersion by continuously increasing the length of the additional SMF step by step (step size: 0.5 m). When the SMF reaches 5 m, and the net cavity dispersion is ~0.18 ps^2, the evolution from DS to DSR is observed as the pump power is successively increased. Figure 5a records the spectral dynamics of the whole process, similar to references [33–35]. At the beginning, when the pump intensity is in the range of ~120–336 mW, the laser operates in a single-DS state, and the spectrum has a rectangular profile with a flat peak and steep edges. As the pump intensity continues to increase (~336–493 mW), the pulse begins to fragment, showing emerging harmonics and chaos. The appearance of continuous components in the corresponding spectrum (spectral thickening), with a strong increase in the central part of the original spectrum and a softening of the edges due to the acquisition of a competitive advantage, is manifested by a gradual bulging at the top of the spectrum and a narrowing of the bandwidth. The pump intensity is then further adjusted from ~493 to 1039 mW, and by slightly adjusting PC and SA, the mode-locking is switched to a single-pulse state; while the spectrum already presents a clear triangular profile. The bandwidth ranges from ~2.76 to 3.81 nm, and the central wavelength is ~1563.25 nm. Figure 5b represents the temporal establishment of the DSR operation, where the pulse profile evolves from a Gaussian to a square case with a maximum duration of up to ~643.33 ps. To determine whether the ML operation is DSR, the AC trace is examined; no fine structure could be observed except for a constant level. For better clarity, we have also implemented a dispersive Fourier transform using 7 km DCF (YOFC, DM1010-E). As expected, the single-shot spectrum (Figure 5c) is in excellent agreement with the averaged spectrum. In this case, no highly structured spectra with drastic fluctuations or pronounced distortions are found, confirming the coherence and that the pulses should be DSR rather than noise-like pulse (NLP) [39–41]. Then, to determine

the upper limit of dispersion, the additional SMF is replaced by DCF, and the length is increased in 0.25 m increments. When the DCF reaches 2.5 m (dispersion: ~0.37 ps^2), the evolution from DS to DSR is also observed as the pump power is successively increased, as shown in Figure 5d. The difference is that, initially, although the spectrum has a flat top, both sides are gently edged, probably due to greater dispersion and weaker filtering. It then undergoes fine structure sub-pulses emergence, free movement, and degradation of ML operation, with the center of the spectrum booming and reconverting to a fundamental RP ML state. At the strongest pumping intensity, the spectrum exhibits a triangular profile with a center wavelength and bandwidth of ~1556.63 and 3.59 nm, respectively. At this point, it can be concluded that the dispersion range in which the DS–ML operation of the present laser can exist stably is approximately 0.18–0.37 ps^2.

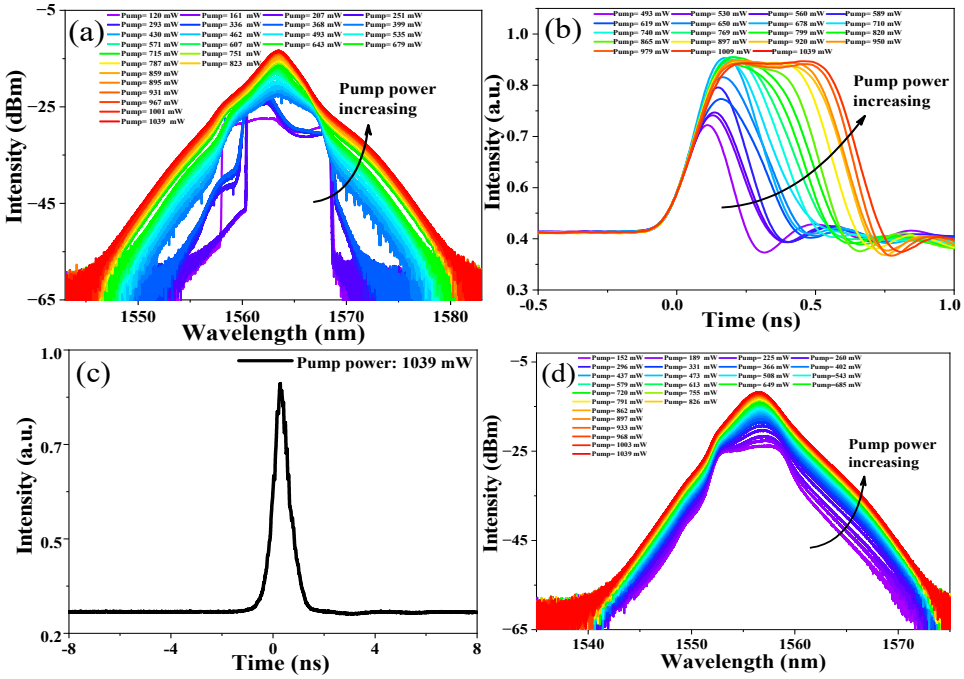


Figure 5. Characteristic dynamics of the ML operation as a function of dispersion. (**a**) The spectrum evolution from DS to DSR operation when additional stretch of the SMF is 5 m; (**b**) the establishment of DSR of temporal profiles; (**c**) the result of DFT; (**d**) the spectrum evolution from DS to DSR operation when additional stretch of the DCF is 2.5 m.

Generally, high nonlinearity or a long cavity facilitates the formation and broadening of the DSR/NLP rectangular pulse (RP) with large dispersion [30,40]. Theoretically, the mechanism of NLMI mode-locking is different from NPR/NALM, both of which require a long fiber to accumulate an appropriate phase shift, which is not the case for NLMI. So, it is interesting and wonderful to study whether the long cavities have a similar effect on RP ML operation in NLMI mode-locked lasers. For this purpose, the additional SMF is extended to ~500 m (net dispersion: ~−10.23 ps^2). By fine-tuning the PC and SAs, the highly stable RP can be achieved beyond 533 mW and could be maintained up to 1039 mW without suffering any pulse break-up. The generated RPs with almost constant peaks and increasing durations are shown in Figure 6a. The inset (top) presents the corresponding pulse train with a ~2.51 µs separation. The AC trace is also examined, no fine structure is found, and together with the DFT result (inset, bottom), the DSR property is identified. Figure 6b plots the spectrum with triangular profiles and bandwidths ranging from ~0.63 to 1.23 nm, centered at ~1558.21–1558.63 nm. As shown in Figure 6c, the RF without satellites has an SNR of ~60.33 dB and is located at ~0.398 MHz (resolution: 100 Hz). The inset is a 300 MHz RF spectrum showing the intrinsic characteristic of DSR with an amplitude modulation period of 109.05 MHz, corresponding to a pulse duration of ~9.17 ns. It can

be seen from Figure 6d that the output power and pulse duration have a quasi-linear rise range of 3.58–12.06 mW and 9.17–32.39 ns, respectively, corresponding to a single pulse energy of 8.99–30.30 nJ. The peak power is almost fixed at a comparable level of ~0.95 W. In particular, a wedge-shaped pulse can be achieved with proper re-adjustment of the PC and SAs when the pump power exceeds 569 mW. Figure 6e presents the dynamics of the temporal evolution with increasing pump power. It can be seen that with increasing pump strength, the amplitude of the pulse is enhanced, the width is broadened, and the maximum duration is ~12 ns. The RF has an SNR of ~53.59 dB (see inset top). The inset (bottom) depicts a pulse train. Figure 6f shows the spectrum with center wavelengths of ~1559.71 nm and bandwidths ranging from ~2.86 to 3.62 nm. According to refs [30,40], the formation mechanism of this wedge-shaped pulse can be attributed to the fact that the leading and trailing edges operate at different positions of the sinusoidal transmittance curve. The above results demonstrate that the long cavity still plays a key role in the RP operation of NLMI, but its broadening efficiency is much lower than that of NPR/NALM. Therefore, the NLMI GIMF–SA-based fiber laser is promising for the generation of high peak DSR/NLP–RP.

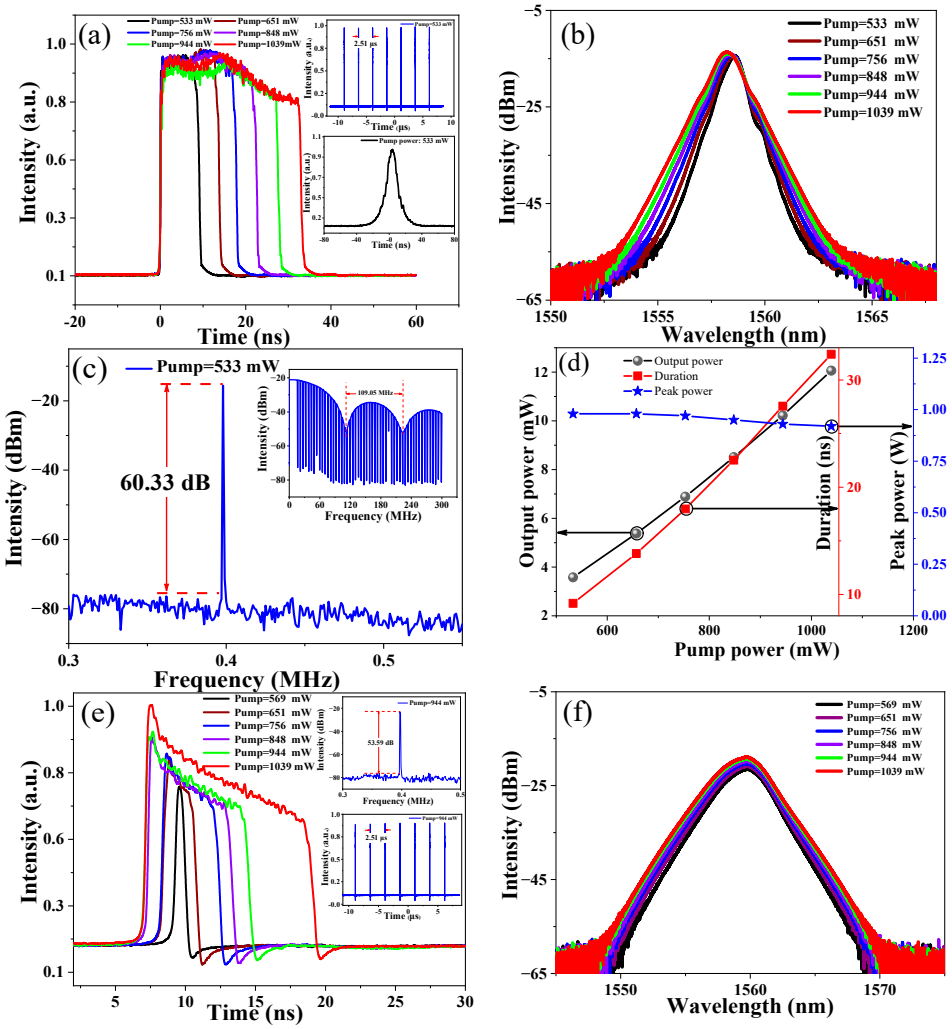


Figure 6. Characteristics of the RP-case ML operations. (**a**) The temporal profiles of DSR ML operation when additional stretch of the SMF is ~500 m. Inset (**top**): a pulse train. Inset (**bottom**): the result of DFT; (**b**) the corresponding spectrum; (**c**) the RF spectrum. Inset: the corresponding RF spectrum for 300 MHz span; (**d**) the output power, pulse duration, and peak power versus the pump power; (**e**) the typical wedge-shaped ML pulse. Inset (**top**): the RF spectrum. Inset (**bottom**): a pulse train; (**f**) the corresponding spectrum.

Surprisingly, if the additional SMF is selected to be ~40 m (dispersion: ~−0.56 ps^2), stable staircase pulse ML operation can be achieved with a pump intensity in the range of 298–1039 mW by carefully adjusting the PC and SA. The dependence of the temporal profiles on the pumping intensity is presented in Figure 7a. Clearly, the staircase pulse contains two rectangularly approximated sub-pulse components with significant differences in amplitude. The left component with the lower peak has gentle edges, while the right one with the higher peak has sharp edges. In addition, there is also an obvious difference in the evolutionary behavior: as the pumping increases, the amplitude of the leading sub-pulse not only increases but also expands its duration; conversely, the width of the trailing sub-pulse widens, yet the peak power remains almost constant (see inset on the right). The inset (left) depicts the pulse train with an absence of amplitude fluctuations and a uniform interval spacing of 347.70 ps. The fundamental peak is located at the repetition rate of 2.878 MHz, as shown in Figure 7b, with an SNR of 61.08 dB, indicating good ML stability. Probably due to the low intensity of the left component, a modulation period of only 101.52 MHz is clearly observed in the 300 MHz RF spectrum (top inset), corresponding to the 9.85 ns higher right sub-rectangular component. The inset (bottom) shows the corresponding spectrum with a certain number of sidebands, centered at ~1558.87–1560.18 nm and with a bandwidth of ~1.95–3.83 nm.

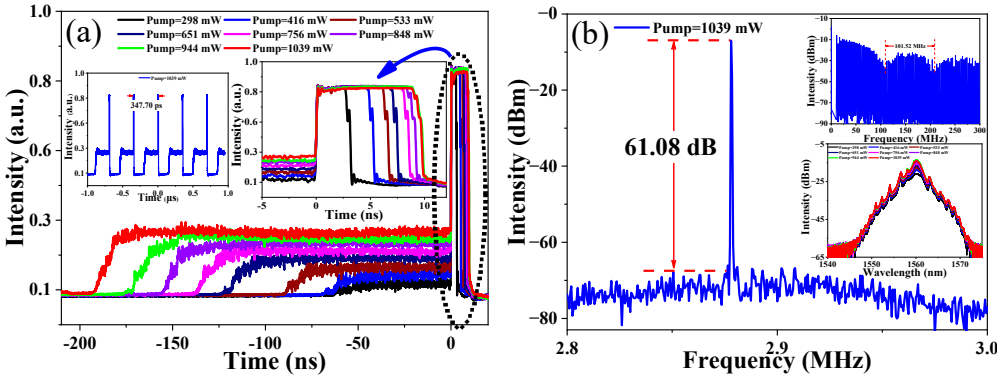


Figure 7. Characteristics of the staircase pulse ML operation. (**a**) The temporal profiles of the staircase ML operation when additional stretch of the SMF is ~40 m. Inset (**left**): a pulse train. Inset (**right**): details of the trailing rectangular portion of the staircase pulse; (**b**) RF spectrum at 1039 mW pump power. Inset (**top**): the RF spectrum for a 300 MHz span. Inset (**bottom**): the optical spectrum.

4. Discussion

Commonly, the usual ML pulses are produced by saturable absorption of an SA, and most NLMI-based studies have focused on this type of property. Conversely, the generation of RP is mainly attributed to the reverse saturation absorption in the transmission. This means that when the pulse intensity reaches this region, it is clamped due to the peak power clamping effect, preventing its amplitude from increasing further and forming a flat peak [10,30]. Unlike previous reports [20–29], the distributed large-core GIMF-based scheme not only facilitates the excitation of more higher-order modes and the removal of the length limitation, but more importantly, it can be beneficial in resisting fragmentation and providing a versatile transfer curve with a wide range of tuning capabilities. In principle, the coupling of two GIMF transfer functions can, under certain conditions, provide richer and more complex properties such as oscillations and associated saturation/reverse saturation absorption phenomena, expansion or contraction of the modulation period, and a wide range of tunability of the modulation depth. In our laser, thanks to the coupled transmission of the distributed GIMF structure, both DS with Gaussian shape, DSR with a typical rectangular profile, and resembling regime with wedge-shaped/staircase pulses are obtained without any additional filter component. These results are summarized in Table 1. The results indicate that, for the first time, we have exploited both the saturable and reverse saturable absorption of the NLMI–SA. According to [10,16,30,40], the formation

mechanism of the wedge/staircase pulses may be attributed to the fact that the leading and trailing parts operate at different positions/stable regions of the modified sinusoidal transmittance curve. Furthermore, the strong amplitude modulation required to form the highly chirped dissipative category pulse must be provided by the distributed GIMF device with filtering properties, implying that the present device acts as both SA and filter [19–21]. It is believed that the performance could be further improved by optimizing the laser cavity; using a double clad gain fiber and a larger pump source. Finally, in order to verify that the mode locking indeed results from the distributed GIMF device, the two GIMFs are deliberately removed from the cavity, and no mode locking can be observed anymore. This verifies that the GIMF structure directly contributes to the mode-locking operation. On the other hand, if any segment of the GIMF is removed, only the DS operation can still be achieved, however, it is less stable, the splitting threshold is significantly reduced, the output single-pulse energy decreases rapidly, and the spectral bandwidth becomes much narrower. The series of comparative experiments show that the coupling and joint operation of two large-core GIMFs are not only beneficial in removing the length limitation, resisting pulse fragmentation, and increasing the single pulse energy, but more interestingly, this scheme provides the opportunity to reconstruct the transmission with sophisticated and intriguing features.

Table 1. Basic parameters of the present distributed GIMF (0.6@0.2 m)-NLMI-based fiber laser.

ML Operation Regime	Dispersion (ps^2)	Region of Transmission	Pump Intensity Range (mW)
DS	~0.28	Saturable	56–1039
DSR	~−10.23	Reverse saturable	533–1039
wedge-shaped	~−10.23	Reverse saturable	569–1039
staircase	~−0.56	Reverse saturable	298–1039

5. Conclusions

In this paper, we have demonstrated a fiber laser based on NLMI-SA using a distributed large-core GIMF structure. This distributed SA device with controllable, widely tunable coupled transmission has the advantage of versatility, flexibility, simple structure, easy construction, non-performance degradation, high damage thresholds, and robustness. Based on this SA, the DS, DSR, wedge-shaped, and staircase ML operations (N = 4) have been experimentally realized without an additional filter. The DS has an output power, pulse energy, bandwidth, and duration of up to 15.33 mW, 2.02 nJ, 22.63 nm, and ~1.68 ps. The DSR has a duration of ~32.39 ns and pulse energy of 30.3 nJ at ~1558.36 nm. The dispersion region (~0.18–0.37 ps^2) that enables DS to exist is investigated, and the dynamics from DS to DSR are observed. Such a simple distributed GIMF–SA structure not only offers a new perspective on all-fiber multifunctional laser sources but may also shed some light on nonlinear science.

Author Contributions: Conceptualization, G.D. methodology, G.D.; S.D.; B.C. and T.W.; software, G.D. and B.L.; validation, Q.Y. and S.D.; formal analysis, S.D.; investigation, G.D.; resources, T.W.; data curation, S.D. and B.L.; writing—original draft preparation, G.D.; writing—review and editing, T.W. and Q.Y.; visualization, B.C. and B.L.; supervision, T.W.; project administration, T.W.; funding acquisition, T.W. and Q.Y. All authors have read and agreed to the published version of the manuscript.

Funding: This research was funded by the Natural Science Foundation of Jilin Province, grant numbers YDZJ202101ZYTS139, 20220508134RC and YDZJ202201ZYTS418), and Chongqing NSF project, grant number CSTB2022NSCQ-MSX1342, and the National Natural Science Foundation of China under Grant, grant numbers 61975021 and 62105042.

Institutional Review Board Statement: Not applicable.

Informed Consent Statement: Not applicable.

Data Availability Statement: All data generated in this study are shown in this manuscript.

Conflicts of Interest: The authors declare no conflicts of interest.

References

1. Fermann, M.E.; Hartl, I. Ultrafast fiber lasers. *Nat. Photonics* **2013**, *7*, 868–874. [CrossRef]
2. Zhang, N.; Song, Q.S.; Zhou, J.J.; Jian, L.; Liu, D.S.; Zhang, H.Y.; Xu, X.D.; Xue, Y.Y.; Xu, J.; Chen, W.D. 44-fs pulse generation at 2.05 μm from a SESAM mode-locked Tm: $GdScO_3$ laser. *Opt. Lett.* **2023**, *48*, 510–513. [CrossRef] [PubMed]
3. Wang, Y.C.; Zhao, Y.G.; Pan, Z.B.; Ban, J.E.; Choi, S.Y.; Rotermund, F.; Loiko, P.; Serres, J.M.; Mateos, X.; Yu, H.H.; et al. 78 fs SWCNT-SA mode-locked Tm: CLNGG disordered garnet crystal laser at 2017 nm. *Opt. Lett.* **2018**, *43*, 4268–4271. [CrossRef] [PubMed]
4. Pawliszewska, M.; Martynkien, T.; Przewloka, A.; Sotor, J. Dispersion-managed Ho-doped fiber laser mode-locked with a graphene saturable absorber. *Opt. Lett.* **2018**, *43*, 38–41. [CrossRef] [PubMed]
5. Liu, H.; Luo, A.P.; Tang, R.; Liu, M.; Luo, Z.C.; Xu, W.C.; Zhao, C.J.; Zhang, H. Femtosecond pulse erbium-doped fiber laser by a few-layer MoS2 saturable absorber. *Opt. Lett.* **2014**, *39*, 4591–4594. [CrossRef]
6. Yan, P.G.; Lin, R.Y.; Ruan, S.G.; Liu, A.J.; Chen, H. A 295 GHz, femtosecond passive harmonic mode-locked fiber laser based on evanescent field interaction with topological insulator film. *Opt. Express* **2015**, *23*, 154–164. [CrossRef]
7. Sotor, J.; Sobon, G.; Kowalczyk, M.; Macherzynski, W.; Paletkoacherzynski, P.; Abramski, M. Ultrafast thulium-doped fiber laser mode locked with black phosphorus. *Opt. Lett.* **2015**, *40*, 3885–3888. [CrossRef]
8. Garside, B.K.; Lim, T.K. Laser mode locking using saturable absorbers. *J. App. Phys.* **1973**, *44*, 2335–2342. [CrossRef]
9. Deng, D.C.; Zhang, H.T.; Zu, J.Q.; Chen, J.Y. Buildup dynamics of pulsating dissipative soliton in an all-normal-dispersion PM Yb-doped fiber laser with NALM. *Opt. Lett.* **2021**, *46*, 1612–1615. [CrossRef]
10. Semaan, G.; Komarov, A.; Niang, A.; Meng, Y.C.; Kemel, M.; Salhi, M.; Sanchez, F. Theoretical and experimental analysis of staircase pulses in passive mode-locked fiber lasers. *Phys. Rev. A* **2018**, *98*, 033819. [CrossRef]
11. Wright, L.G.; Christodoulides, D.N.; Wise, F.W. Spatiotemporal mode-locking in multimode fiber lasers. *Science* **2017**, *358*, 94–97. [CrossRef]
12. Eftekhar, M.A.; Sanjabi-Eznaveh, Z.; Lopez-Aviles, H.; Benis, S.; Antonio-Lopez, J.E.; Kolesik, M.; Wise, F.; Amezcua-Correa, R.; Christodoulides, D.N. Accelerated nonlinear interactions in graded-index multimode fibers. *Nat. Commun.* **2019**, *10*, 1638. [CrossRef]
13. Mafi, A. Pulse Propagation in a Short Nonlinear Graded-Index Multimode Optical Fiber. *J. Light. Technol.* **2012**, *30*, 2803–2811. [CrossRef]
14. Nazemosadat, E.; Mafi, A. Nonlinear multimodal interference and saturable absorption using a short graded-index multimode optical fiber. *J. Opt. Soc. Am. B* **2013**, *30*, 1357–1367. [CrossRef]
15. Wang, Z.K.; Chen, J.K.; Zhu, T.N.; Wang, D.N.; Gao, F. Graded index fiber as an all-fiber saturable absorber for large energy conventional soliton and dissipative soliton generation. *Photonics Res.* **2019**, *7*, 1214–1220. [CrossRef]
16. Chen, G.W.; Li, W.L.; Wang, G.M.; Zhang, W.F.; Zeng, C.; Zhao, W. Generation of coexisting high-energy pulses in a mode-locked all-fiber laser with a nonlinear multimodal interference technique. *Photonics Res.* **2019**, *7*, 187–192. [CrossRef]
17. Chen, T.; Zhang, Q.L.; Zhang, Y.P.; Li, X.; Zhang, H.K.; Xia, W. All-fiber passively mode-locked laser using nonlinear multimode interference of step-index multimode fiber. *Photonics Res.* **2018**, *6*, 1033–1039. [CrossRef]
18. Luo, Y.Y.; Yang, X.; Shum, P.P.; Liu, Y.S.; Xia, R.; Ni, W.J.; Lam, H.Q.; Sun, Q.Z.; Tang, X.H. Stationary and pulsing vector dissipative solitons in nonlinear multimode interference-based fiber lasers. *Opt. Express* **2020**, *28*, 4216–4224. [CrossRef] [PubMed]
19. Chen, J.K.; Wang, Z.K.; Li, L.J.; Wang, D.N.; Zhu, T.Y.; Gao, F.; Cao, S.Y.; Fang, Z.J. GIMF-Based SA for Generation of High Pulse Energy Ultrafast Solitons in a Mode-Locked Linear-Cavity Fiber Laser. *J. Light. Technol.* **2019**, *38*, 1480–1485. [CrossRef]
20. Chang, S.; Wang, Z.K.; Wang, D.N.; Zhu, T.Y.; Hua, K.; Gao, F. Tunable and dual-wavelength mode-locked Yb-doped fiber laser based on graded-index multimode fiber device. *Opt. Laser Technol.* **2021**, *140*, 107081. [CrossRef]
21. Teğin, U.; Ortaç, B. All-fiber all-normal-dispersion femtosecond laser with nonlinear multimodal interference based saturable absorber. *Opt. Lett.* **2018**, *43*, 1611–1614. [CrossRef] [PubMed]
22. Wang, Z.K.; Wang, D.N.; Yang, F.; Li, L.; Zhao, C.; Xu, B.; Jin, S.; Cao, S.; Fang, Z. Er-Doped Mode-Locked Fiber Laser with a Hybrid Structure of a Step-Index-Graded-Index Multimode Fiber as the Saturable Absorber. *J. Light. Technol.* **2017**, *35*, 5280–5285. [CrossRef]
23. Li, H.H.; Wang, Z.K.; Li, C.; Zhang, J.J.; Xu, S.Q. Mode-locked Tm fiber laser using SMF-SIMF-GIMF-SMF fiber structure as a saturable absorber. *Opt. Express* **2017**, *25*, 26546–26553. [CrossRef] [PubMed]
24. Li, H.H.; Wang, Z.K.; Li, C.; Tian, Y.; Xiao, Z.; Zhang, J.J.; Xu, S.Q. Self-starting mode-locked Tm-doped fiber laser using a hybrid structure of no core-graded index multimode fiber as the saturable absorber. *Opt. Laser Technol.* **2019**, *113*, 317–321. [CrossRef]
25. Harith, A.; Mansor, N.H.; Samion, M.Z.; Reduan, S.A. High power mode-locked erbium-ytterbium doped fiber laser using GIMF-SIMF-GIMF fiber structure as saturable absorber. *Opt. Quantum Electron.* **2023**, *55*, 213.

26. Yang, F.; Wang, D.N.; Wang, Z.K.; Li, L.J.; Zhao, C.L.; Xu, B.; Jin, S.Z.; Cao, S.Y.; Fang, Z.J. Saturable absorber based on a single mode fiber-graded index fiber-single mode fiber structure with inner micro-cavity. *Opt. Express* **2018**, *26*, 927–934. [CrossRef] [PubMed]
27. Wang, Z.K.; Wang, D.N.; Yang, F.; Li, L.J.; Zhao, C.L.; Xu, B.; Jing, S.Z.; Cao, S.Y.; Fang, Z.J. Stretched graded-index multimode optical fiber as a saturable absorber for erbium-doped fiber laser mode locking. *Opt. Lett.* **2018**, *43*, 2078–2081. [CrossRef] [PubMed]
28. Wang, Z.K.; Li, L.J.; Wang, D.N.; Le, Z.C.; Zhang, S.Q.; Cao, S.Y.; Fang, Z.J. Generation of pulse-width controllable dissipative solitons and bound solitons by using an all-fiber saturable absorber. *Opt. Lett.* **2019**, *44*, 570–573. [CrossRef] [PubMed]
29. Li, H.H.; Hu, F.M.; Tian, Y.; Wang, P.T.; Zhang, J.J.; Xu, S.Q. Continuously wavelength-tunable mode-locked Tm fiber laser using stretched SMF-GIMF-SMF structure as both saturable absorber and filter. *Opt. Express* **2019**, *27*, 14437–14446. [CrossRef]
30. Dong, Z.P.; Lin, J.Q.; Li, H.X.; Li, S.J.; Tao, R.X.; Gu, C.; Yao, P.J.; Xu, L.X. Generation of mode-locked square-shaped and chair-like pulse based on reverse saturable absorption effect of nonlinear multimode interference. *Opt. Express* **2019**, *27*, 27610–27617. [CrossRef]
31. Zhang, K.X.; Rochette, M. All-fiber Saturable Absorber Using Nonlinear Multimode Interference in a Chalcogenide Fiber. *J. Light. Technol.* **2020**, *38*, 6321–6326. [CrossRef]
32. Zhang, H.G.; Jin, L.; Zhang, H.; Xu, Y.G.; Shi, L.L.; Wang, T.B.; Chen, H.L.; Wang, D.T.; Ma, X.H. All-fiber nonlinear optical switch based on polarization controller coiled SMF-GIMF-SMF for ultrashort pulse generation. *Opt. Commun.* **2019**, *452*, 7–11. [CrossRef]
33. Chang, W.; Ankiewicz, A.; Soto-Crespo, J.-M.; Akhmediev, N.N. Dissipative soliton resonances in laser models with parameter management. *J. Opt. Soc. Am. B* **2008**, *25*, 1972–1977. [CrossRef]
34. Komarov, A.; Amrani, F.; Dmitriev, A.; Komarov, K.; Sanchez, F. Competition and coexistence of ultrashort pulses in passive mode-locked lasers under dissipative-soliton-resonance conditions. *Phys. Rev. A* **2013**, *87*, 023838. [CrossRef]
35. Cheng, Z.C.; Li, H.H.; Wang, P. Simulation of generation of dissipative soliton, dissipative soliton resonance and noise-like pulse in Yb-doped mode-locked fiber lasers. *Opt. Express* **2015**, *23*, 5972–5981. [CrossRef] [PubMed]
36. Wang, D.Y.; Yi, Z.; Ma, G.L.; Dai, B.; Yang, J.B.; Zhang, J.F.; Yu, Y.; Liu, C.; Wu, X.; Bian, Q. Two channels photonic crystal fiber based on surface plasmon resonance for magnetic field and temperature dual-parameter sensing. *Phys. Chem. Chem. Phys.* **2022**, *24*, 21233–21241. [CrossRef] [PubMed]
37. Wang, D.Y.; Zhu, W.L.; Yi, Z.; Ma, G.L.; Gao, X.; Dai, B.; Yu, Y.; Zhou, G.R.; Wu, P.H.; Liu, C. Highly sensitive sensing of a magnetic field and temperature based on two open ring channels SPR-PCF. *Opt. Express* **2022**, *30*, 39055–39067. [CrossRef] [PubMed]
38. Zhu, W.L.; Yi, Y.T.; Yi, Z.; Bian, L.; Yang, H.; Zhang, J.G.; Yu, Y.; Liu, C.; Li, G.F.; Wu, X.W. High confidence plasmonic sensor based on photonic crystal fibers with a U-shaped detection channel. *Phys. Chem. Chem. Phys.* **2023**, *5*, 8583–8591. [CrossRef] [PubMed]
39. Kemel, M.; Salhi, M.; Ciret, C.; Semaan, G.; Nady, N.; Sanchez, F. Coherence characterization of nanosecond rectangular pulses in passively mode-locked fiber lasers. *OSA Contin.* **2021**, *4*, 279–289. [CrossRef]
40. Deng, G.; Yang, Q.C.; Du, S.L.; Chen, B.W.; Li, B.Q.; Wang, T.S. Three-step staircase-like pulses generation in a butterfly-shaped mode-locked fiber laser. *Opt. Commun.* **2023**, *543*, 129604. [CrossRef]
41. Runge, A.F.J.; Aguergaray, C.; Broderick, N.G.R.; Erkintalo, M. Coherence and shot-to-shot spectral fluctuations in noise-like ultrafast fiber lasers. *Opt. Lett.* **2013**, *38*, 4327–4330. [CrossRef] [PubMed]

Disclaimer/Publisher's Note: The statements, opinions and data contained in all publications are solely those of the individual author(s) and contributor(s) and not of MDPI and/or the editor(s). MDPI and/or the editor(s) disclaim responsibility for any injury to people or property resulting from any ideas, methods, instructions or products referred to in the content.